Surface Phase Nucleation of Lead Monoatomic Layers on Si(111) Induced by Manganese Phthalocyanine Molecules

Danilo Longo, Marie-Laure Bocquet, Nicolás Lorente, Hervé Cruguel, François Debontridder, Sébastien Royer, Pascal David, Alexandra Palacio-Morales, Tristan Cren, Nadine Witkowski, et al.

Surface Phase Nucleation of Pb Monoatomic Layers on Si(111) Induced by Manganese-Phthalocyanine Molecules

Danilo Longo,[*,†,‡] Marie-Laure Bocquet,[¶] Nicolás Lorente,[§,‖] Hervé Cruguel,[†] François Debontridder,[†] Sébastien Royer,[†] Pascal David,[†] Alexandra Palacio-Morales,[†] Tristan Cren,[†] Nadine Witkowski,[†] and Christophe Brun[†]

†*Sorbonne Université, CNRS, Institut des Nanosciences de Paris, UMR7588, F-75252, Paris, France*

‡*Synchrotron SOLEIL, L'Orme des Merisiers, Saint-Aubin, 91190, France*

¶*PASTEUR, Département de Chimie, École Normale Supérieure, Sorbonne Université, CNRS, 75005 Paris, France*

§*Centro de Física de Materiales CFM/MPC (CSIC-UPV/EHU), 20018 Donostia-San Sebastián, Spain*

‖*Donostia International Physics Center (DIPC), 20018 Donostia-San Sebastián, Spain*

E-mail: danilo.longo@synchrotron-soleil.fr

Abstract

Hybrid interfaces where organic molecules are adsorbed on metallic substrates are very interesting to understand the fundamental interactions that might modify the chemical-physical properties of molecules or substrate. Here, we explore the adsorption of manganese phthalocyanines (MnPcs) on different structural phases of a Pb monoatomic layer, namely the $\sqrt{7} \times \sqrt{3}$-Pb and the Striped Incommensurate phase (SIC-Pb) phase, grown on Si(111). Surprisingly, the deposition of a minute amount of MnPc molecules ($\sim$0.18 molecules/100 nm^2) nucleates a macroscopic structural transition of the $\sqrt{7} \times \sqrt{3}$-Pb phase into the SIC-Pb phase. Our combined Scanning Tunneling Microscopy, Low Energy Electron Diffraction and Density Functional Theory study revealed that the mechanism behind this surface transformation is related to a strong and local molecule-substrate interaction. The structural phase transition is finally driven by the strained nature of the Pb phases and the energetic stability of the MnPc/SIC-Pb/Si(111) system with respect to MnPc/$\sqrt{7} \times \sqrt{3}$-Pb/Si(111) one. The molecule-substrate interaction found in the present study is stronger than the one observed on Pb(111) bulk or thin films, highlighting the implication of the Pb/Si(111) interface in the interaction process. Hence, our results reveal that playing with the substrate dimensionality to tune the molecule-substrate coupling has strong impact on the electronic/magnetic properties of organic hybrid systems.

Abbreviations

MPc=metal-phthalocyanine

T_C= superconducting temperature

TTCNQ=7,7,8,8-tetracyanoquinodimethane

SMON=surface metal-organic network

STM=scanning tunneling microscopy

LEED=low energy electron diffraction

DFT=density functional theory

SIC=striped incommensurate phase

2D= two dimensional

3D= three dimensional

ML=monolayer

PDOS= projected density of states

UHV=ultra-high vacuum

Keywords

surface phase transition, metal/semiconductor interface, lead monolayer, molecule-substrate interaction, phthalocyanines, two-dimensional metallic systems, molecular electronic/magnetic properties

Introduction

The recent search for topological superconductivity[1] prompted intense efforts to study the basic coupling between magnetic impurities and superconducting materials.[2–5] Recently, it has been shown that this coupling strongly depends on the dimensionality of the superconductor[6] and that 2D materials might be much more promising than 3D ones for such purpose.[7–9] In this regard, metallic monolayers of either Pb or In epitaxially grown on semiconducting substrates constitute a very interesting class of systems.[10–12] Moreover, coupling these 2D materials with arrays of metallo-organic molecules, *e.g.* metal-phthalocyanines (MPcs), seems an appealing way to realize hybrid magnetic/superconducting systems.

One of the advantages of using MPcs is the possibility of tailoring the molecule-substrate coupling by selecting the most appropriate metallic atom M to coordinate within the molecular structure.[13] For this reason the interaction of MPcs with different substrates has been extensively investigated.[14–19] Interestingly, the set of these studies reveals that, in addition to the coordinated atom M, the substrate also plays a crucial role in balancing the relative

strength of the molecule-molecule and molecule-substrate interaction. As an example, it has recently been shown that MPcs deposited on the $\sqrt{7}\times\sqrt{3}$-In phase of the In/Si(111) bilayer form closely packed square lattices[19] indicating the prevalence of the molecule-molecule interaction. As small as it is, the molecule-substrate interaction remains non-negligible since the critical superconducting temperature (T_C) of the In bilayer increases or decreases according to the particular MPc (M=Mn or Cu) deposited on the surface.

If self-assembly of MPcs on the In bilayer results in square lattices, the adsorption of molecules that interact more strongly with the substrate might lead to very different behavior of the hybrid system. For instance, the deposition of 7,7,8,8-tetracyanoquinodimethane (TCNQ) molecules on top of the $\sqrt{7}\times\sqrt{3}$-In/Si(111) bilayer leads to the formation of a surface metal-organic network (SMON) with inclusion of In atoms extracted from the underlying metallic substrate.[20] Simultaneously, the metallic area surrounding the SMON undergoes a surface reconstruction from the $\sqrt{7}\times\sqrt{3}$-In phase to a novel 5×5-In phase as a consequence of the local decrease in In coverage. Surface reconstruction of a 2D metallic system induced by molecular adsorption was also reported by Matetskiy *et al.*[21] In that study, C_{60} molecules were deposited on top of the $\sqrt{7}\times\sqrt{3}$-Pb phase of the Pb/Si(111) monolayer. Self-assembly of disordered C_{60} islands was accompanied by the expulsion of Pb atoms from the monolayer allowing the molecular domains to be incorporated within the layer. Expelled Pb atoms were subsequently reintegrated in the regions surrounding the C_{60} islands by increasing the local Pb coverage thus leading to a structural phase transition of the Pb surface from the $\sqrt{7}\times\sqrt{3}$-Pb to the denser hexagonal incommensurate HIC phase.

Here, we report on a combined Scanning Tunneling Microscopy (STM), Low Energy Electron Diffraction (LEED) and Density Functional Theory (DFT) study on the properties of crystalline Pb monolayers grown on Si(111) in presence of minute concentrations of manganese phthalocyanines (MnPcs). We present a new structural phase transition of the Pb/Si(111) monolayer, from the $\sqrt{7}\times\sqrt{3}$-Pb/Si(111) to the Striped Incommensurate (SIC) phase, taking place upon adsorption of $\sim$0.18 molecules/100 nm^2 of MnPcs. In contrast to previous studies

on similar systems, we found that the surface reconstruction mechanism does not imply the expulsion/reintegration of Pb atoms close to the molecules but is rather related to the strong local molecule-substrate interaction. The structural transition is ultimately promoted by the strained nature of the Pb phases and the energetic stability of the MnPc/SIC-Pb/Si(111) system compared to the MnPc/$\sqrt{7}\times\sqrt{3}$-Pb/Si(111). Moreover, LEED measurements reveal that $\sim$0.18 molecules/100 nm^2 of MnPcs are already able to nucleate the new phase. This molecule-induced surface reconstruction as well as the observation of a frustrated molecular self-assembly reflecting the threefold symmetry of the substrate reveal an enhanced molecule-substrate coupling stronger than what is known on bulk or ultrathin Pb substrates. This is corroborated by our DFT calculations showing that the Pb/Si(111) interface plays a crucial role in determining the molecule-substrate coupling strength as well as the physical properties of the system such as the magnetic state of the MnPc molecules. Ultimately, our results emphasize the rich and new behavior of hybrid organic/metal systems emerging when the dimensionality of the metallic substrate is reduced. In particular, this could enable a new way of tuning the coupling between magnetic molecules and a 2D superconductor, with the aim of stabilizing well-defined magnetic ordering of the molecular array.

Results and discussion

Experimental results

The adsorption of MnPc molecules on Pb monolayers was carried out after proper preparation of the substrate. Single atomic layers of lead were obtained by first depositing 1.65 monolayer (ML) of Pb on top of a freshly annealed Si(111) surface with 7×7 reconstruction. Then, the sample was annealed at about 600 K for a few minutes. Finally, the crystalline quality of the Pb/Si(111) surface was checked with both STM and LEED (see Methods section for details). Figure 1a shows STM and LEED results of the $\sqrt{7}\times\sqrt{3}$-Pb surface before MnPcs deposition that develops below 270 K as a result of a reversible temperature-induced structural phase

transition.[22–29] The $\sqrt{7}\times\sqrt{3}$-Pb phase, that covers the entire sample surface, is not a single domain phase but it consists of three equivalent domains 120° mutually rotated and with an average size of about 100×100 nm^2.[30–33] Accordingly, the complex LEED pattern of Figure 1a is due to the overlap of the diffraction spots arising from the Si(111)-1×1 substrate and the three $\sqrt{7}\times\sqrt{3}$-Pb domains (one of them is highlighted by the purple arrows).[27,34,35] The STM image of figure 1a shows only one of these $\sqrt{7}\times\sqrt{3}$-Pb domains and reveals the typical periodic arrangement of Pb atoms in straight lines.[24–26,28] The $\sqrt{7}\times\sqrt{3}$-Pb unit cell contains 6 Pb atoms per 5 Si atoms corresponding to a Pb coverage of $\frac{6}{5}$ ML=1.2 ML.[25,29,31,33,35,36]

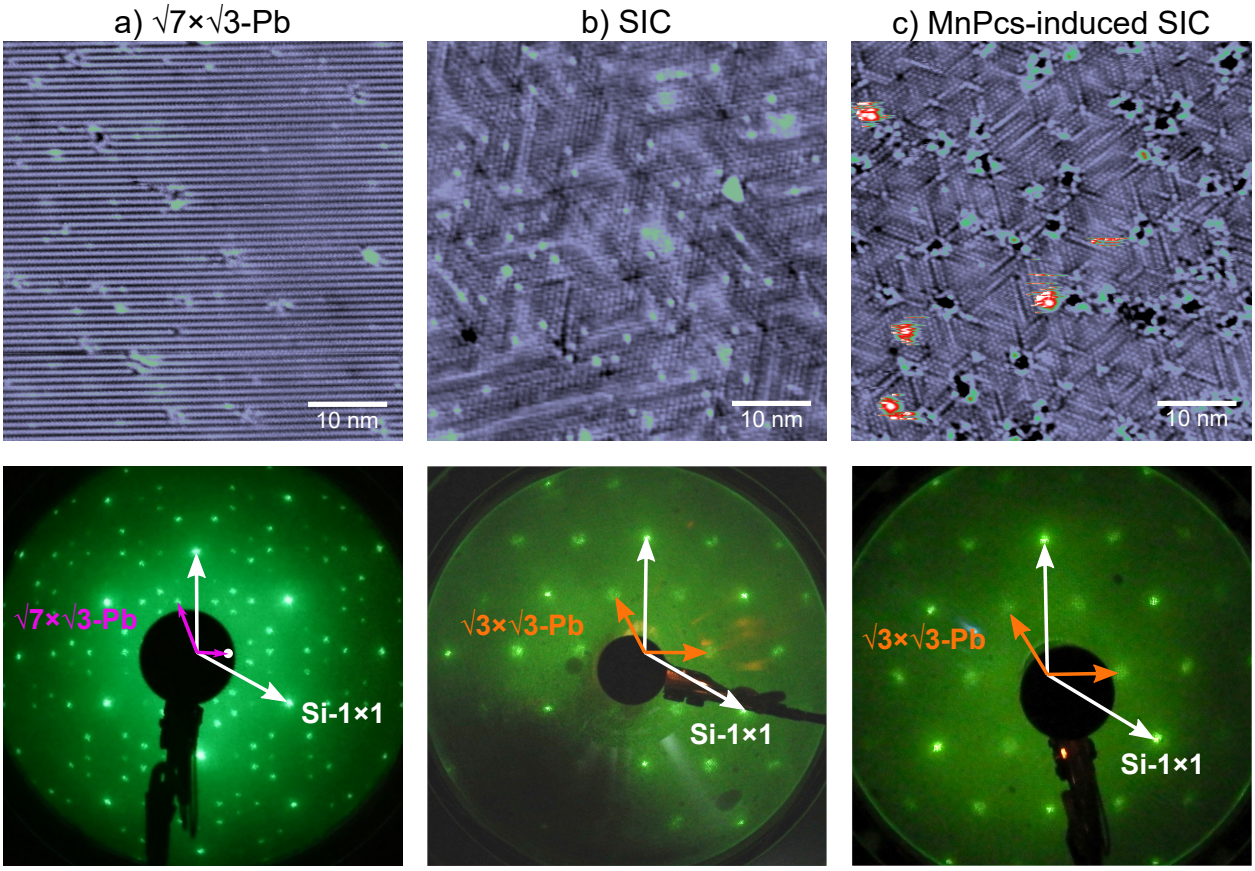

Figure 1: (a) and (b) show STM images (top) and LEED patterns (bottom) of a Pb/Si(111) monolayer prepared in the $\sqrt{7}\times\sqrt{3}$-Pb and SIC phase respectively. (c) shows the STM image (top) and the LEED pattern (bottom) of the SIC reconstruction induced by adsorption of ∼0.18 molecules/100 nm^2 of MnPcs on the Pb monolayer initially prepared in the $\sqrt{7}\times\sqrt{3}$-Pb phase (substrate kept at room temperature during MnPcs deposition). All STM images were measured at 77 K over a 50×50 nm^2 area: (a) V_T=+1 V / I_T=20 pA, (b) V_T=-50 mV / I_T=80 pA and (c) V_T=+0.1 V / I_T=40 pA. Corresponding LEED patterns recorded at E∼80 eV and (a) 100 K (b) 300 K (c) 100 K.

Figure 1b shows STM and LEED results of the Striped Incommensurate phase (SIC) which is the densest phase of the Pb monoatomic layer obtained at the saturation coverage of 1.3 ML.[27,37] Here, it should be stressed the fact that, unlike the $\sqrt{7}\times\sqrt{3}$-Pb phase, the SIC phase does not undergo structural changes from room temperature to low temperature.[27] The analysis of STM images reveals that the incommensurate structure of this phase consists of small $\sqrt{3}\times\sqrt{3}$-Pb domains (brighter regions) separated by meandering domain walls with quasi-$\sqrt{7}\times\sqrt{3}$-Pb atomic arrangements (dark stripes).[22,27,37–40] According to this, the LEED pattern of Figure 1b shows the $\sqrt{3}\times\sqrt{3}$-like symmetry of the SIC phase (indicated by orange arrows) superimposed to the 1×1 pattern of the Si(111) substrate.[34,38] Previous detailed studies have shown that the superstructure spots of the SIC phase located around the $\sqrt{3}\times\sqrt{3}$ positions contain information on the incommensurate nature of this surface.[27,35] A Pb monoatomic layer with a pure commensurate $\sqrt{3}\times\sqrt{3}$-Pb phase would have a unit cell with 4 Pb atoms per 3 Si atoms corresponding to a Pb coverage of $\frac{4}{3}$ ML=1.33 ML.[22,34,38,41,42] However, due to the large lattice mismatch between the Pb(111) and Si(111) surfaces, *i.e.* a_{Pb}=4.92 Å and a_{Si}=5.43 Å, a pure $\sqrt{3}\times\sqrt{3}$-Pb atomic arrangement would require a compression of the Pb monoatomic layer of about 5%.[10,38] This is probably too large and may explain why the commensurate $\sqrt{3}\times\sqrt{3}$-Pb surface reconstruction is not experimentally observed whereas the incommensurate SIC phase is observed instead.[34,38] Ultimately, the presence of domain walls with "lighter" quasi-$\sqrt{7}\times\sqrt{3}$-Pb structure leads to a saturation Pb coverage of the SIC phase of 1.3 ML which is slightly less than 1.33 ML of the commensurate $\sqrt{3}\times\sqrt{3}$-Pb.[22,27,34,37,38]

The main result of the present study is depicted in figure 1c. It shows the effect of MnPc deposition on top of the Pb/Si(111) monoatomic layer kept at room temperature and prepared with 1.2 ML of Pb, *i.e.* exhibiting the $\sqrt{7}\times\sqrt{3}$-Pb phase shown in figure 1a below 270 K. The STM image of figure 1c shows that adsorption of ∼0.18 molecules/100 nm^2 of MnPc is sufficient to induce a structural phase transition of the initial $\sqrt{7}\times\sqrt{3}$-Pb surface. Due to molecular motion at 77 K under the STM tip, MnPc molecules appear as bright dis-

continuous protrusions. Remarkably, the LEED pattern of figure 1c shows that the surface reconstruction takes place on a macroscopic scale.

Careful inspection of the STM image of figure 1c and comparison with that of figure 1b reveal that the MnPc-induced surface reconstruction closely resembles the SIC phase. In particular, the alternation of $\sqrt{3}\times\sqrt{3}$-Pb domains (brighter regions) and "almost" $\sqrt{7}\times\sqrt{3}$-Pb domain walls (dark stripes), typical pattern of the SIC phase, can be easily recognized in figure 1c. Moreover, the triangular lattice parameter of 0.67±0.06 nm measured over the brighter regions of the STM image in figure 1c is compatible with that expected for the $\sqrt{3}\times\sqrt{3}$-Pb structure. Same conclusion is derived by the inspection of LEED pattern of figure 1c. That is, after MnPcs adsorption, the initial commensurate diffraction pattern of the $\sqrt{7}\times\sqrt{3}$-Pb surface is replaced by a new lattice of incommensurate spots with $\sqrt{3}\times\sqrt{3}$-like symmetry (indicated by orange arrows) similar to that observed on the SIC phase (compare with the LEED pattern of figure 1b).

It is worth noting that, contrary to what is commonly observed on the pristine SIC phase, irregularly shaped hole-defects with decorated edges are uniformly distributed over the MnPc-induced SIC phase (compare STM images in figure 1b and figure 1c). The emergence of these hole-defects can be easily understood as a compression of the Pb monolayer triggered by MnPcs adsorption. Indeed, the transition from the $\sqrt{7}\times\sqrt{3}$-Pb to the SIC phase usually occurs by increasing the Pb coverage from 1.2 ML to 1.3 ML or equivalently by increasing the surface atomic density from $n_{\sqrt{7}\times\sqrt{3}}$=9.40 atoms/nm^2 to n_{SIC}=10.19 atoms/nm^2.[10,27] On the other hand, our experiments were performed at constant surface Pb coverage. This leads Pb atoms initially arranged in a $\sqrt{7}\times\sqrt{3}$-Pb structure to reorganize themselves into the SIC phase where irregular hole-defects appear then all over the surface because of the conservation of the total number of Pb atoms.

Adsorption of MnPcs at lower substrate temperatures also induced the SIC phase. Figure 2a and figure 2b show MnPc molecules deposited on the $\sqrt{7}\times\sqrt{3}$-Pb phase kept at about 150 K with coverages of ∼0.7 molecules/100 nm^2 and ∼4.6 molecules/100 nm^2 re-

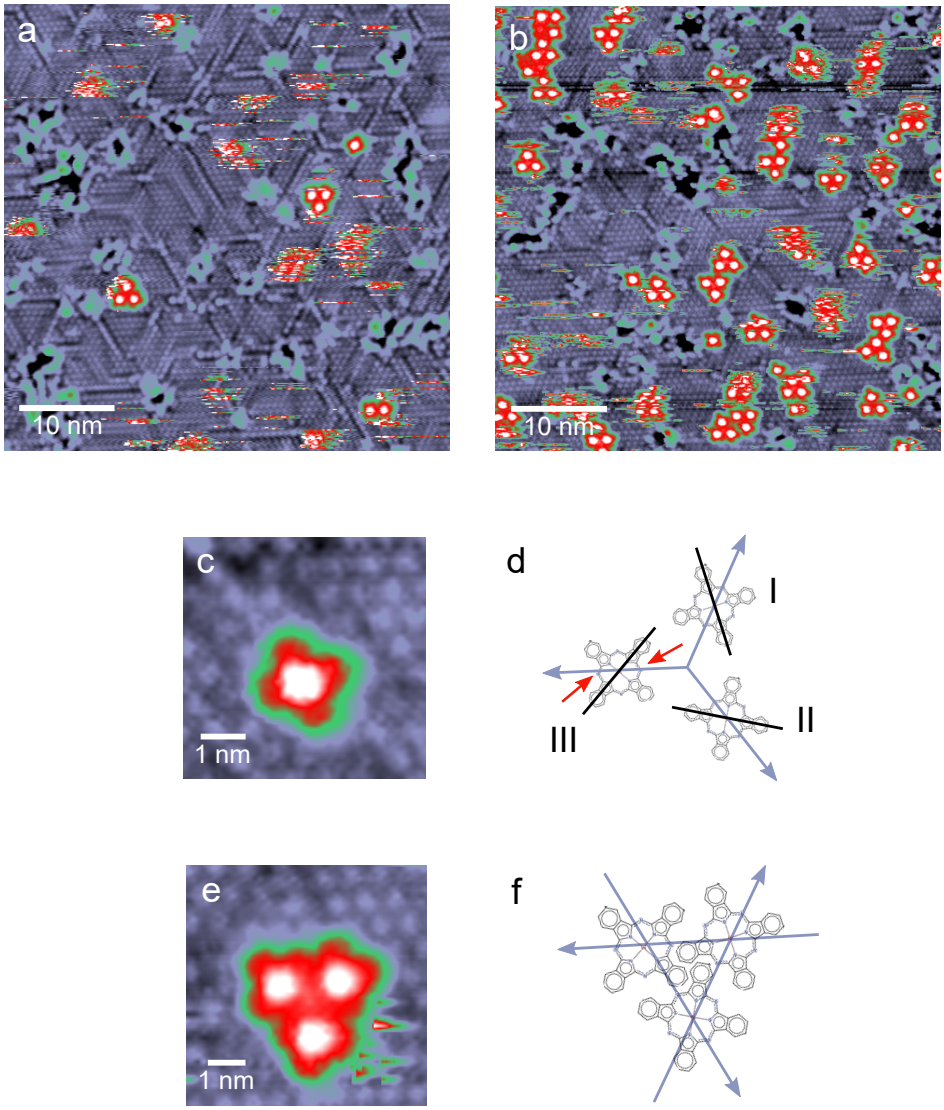

Figure 2: 46×46 nm^2 STM images in (a) and (b) (V_T=+0.3 V and I_T=20 pA and V_T=+0.4 V and I_T=80 pA respectively) show ∼0.7 molecules/100 nm^2 and ∼4.6 molecules/100 nm^2 of MnPcs respectively adsorbed on the MnPcs-induced SIC surface. MnPcs were deposited on the $\sqrt{7} \times \sqrt{3}$-Pb surface kept at approximately 150 K. The 5×5 nm^2 high-resolution STM image (V_T=+0.4 V and I_T=80 pA) in (c) shows a single MnPc molecule corresponding to the configuration I in the sketch (d). The schematic drawing in (d), deduced from the experimental data, represents the three adsorption orientations of single MnPcs with respect to the Pb surface (purple arrows). Red arrows indicate the two nitrogen atoms within MnPcs through which a substrate direction passes. Black segments highlight one of the main molecular axis of a MnPc in a given configuration. The 6×6 nm^2 high-resolution STM image (V_T=+0.5 V and I_T=50 pA) in (e) shows MnPcs self-assembled in a trimer. The relative orientation of a timer with respect to the substrate is depicted in the drawing (f). All STM images were acquired at 77 K at which temperature tip induced molecular motion exists.

spectively. A clear MnPcs-induced SIC reconstruction is observed in both cases. Moreover, one sees that isolated molecules and self-assembled trimers are the most common configurations observed at low molecular densities. Remarkably, this self-assembly behavior of MnPc molecules on the Pb monolayer seem to be independent of the substrate temperature in the range $100 < T < 300$ K. This observation suggests that molecules do diffuse during adsorption and that their final conformations are not limited by diffusion barriers. Our study also reveals that, at low molecular coverage, MnPcs do not self-assemble to form extended long-range ordered molecular arrays on Pb/Si(111) monolayers. This is in contrast to the spontaneous assembly of squared lattices of MnPcs usually observed on Pb thin films or bulk monocrystals.[14–19,43] Moreover, to our knowledge, trimer arrangement of MnPcs has not been previously reported.[14–16,18,19] Furthermore, in contrast to what has been previously reported in the case of C_{60} molecules deposited on the Pb/Si(111) monolayer,[21] MnPc molecules lie on defect-free regions.

Not only do the molecules remain isolated or arranged in trimers, but they present precise orientations with respect to the substrate. Figure 2c displays an isolated MnPc molecule adsorbed on the Pb monolayer surface. The sketch of figure 2d, resulting from statistical analysis of several STM images, shows that isolated MnPcs can be found in only three possible orientations, rotated by an angle of 120° between each other, with respect to the symmetry directions of the Pb monolayer (indicated by purple arrows). The MnPc molecule in figure 2c, for instance, corresponds to the configuration I depicted in figure 2d. For each of these molecular configurations one of the substrate directions is always aligned with the axis passing through the two nitrogen atoms indicated by the red arrows (see figure 2d) within the experimental error of about 2°. All these results and considerations indicate a strong and local influence of the Pb monolayer on the adsorption configuration of MnPcs. This is in stark contrast with the lack of surface registry found for MnPcs adsorption on the (111) surface of bulk Pb[15,16,43] or Pb thin films.[14]

The sketch of figure 2f, deduced from a statistical analysis of STM images, depicts the

arrangement of MnPcs inside self-assembled trimers. The registry of the trimer with respect to the Pb surface high-symmetry directions is indicated by purple arrows. One measured trimer is presented in figure 2e. Comparison between figure 2d and figure 2f reveals that the single MnPcs inside a trimer always retain the same orientation with respect to the Pb substrate as do isolated molecules. More interestingly, all trimers observed in our experiments always consisted of MnPc molecules with the three possible orientations depicted in figure 2d. Figure 2f also shows that each Pb direction passes through Mn atoms of neighboring MnPcs within the experimental error of about 2°. Moreover, these Mn atoms constitute the vertices of an equilateral triangle whose sides (Mn-Mn distance) have a length of 1.46±0.06 nm. These various observations lead us to the conclusion that the Pb/Si(111) monolayer plays an important role in determining the self-assembly properties of MnPc trimers suggesting the presence of strong and directional molecule-substrate interactions in this system.

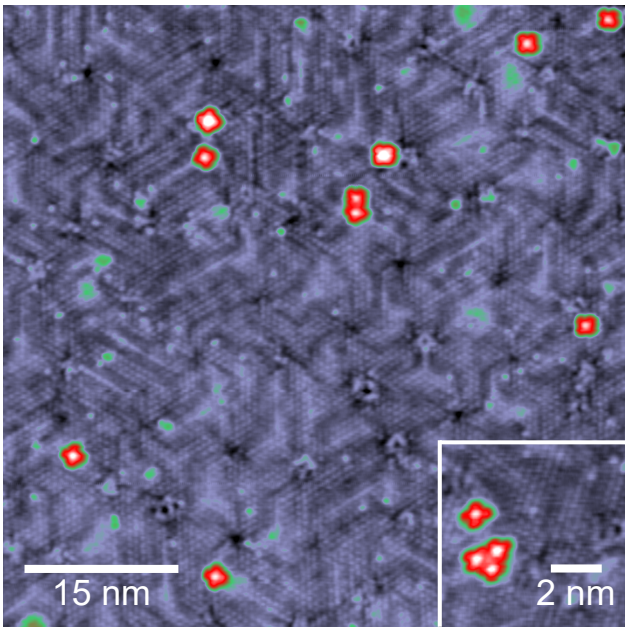

Figure 3: 60×60 nm^2 STM image (V_T=-50 mV and I_T=50 pA) showing ∼1.3 molecules/100 nm^2 of MnPcs deposited on top of the pristine SIC phase of the Pb/Si(111) monolayer kept at room temperature. MnPcs remain isolated or self-assemble in trimers (see inset: 7×7 nm^2, V_T=-50 mV and I_T=50 pA). Both images were measured at 300 mK.

Similar molecular organization was also found on the pristine SIC surface. Figure 3 shows

$\sim$1.3 molecules/100 nm^2 of MnPcs deposited on the SIC phase kept at room temperature. Here the SIC surface structure is not affected by MnPcs adsorption. However, MnPcs retain the same self-assembly properties than the ones observed on the MnPcs-induced SIC phase, that is single MnPcs and self-assembled trimers are the only molecular configurations observed on the Pb monolayer surface (see inset of figure 3) and their arrangement reflects the threefold symmetry of the Pb substrate. Figure 3 also show a dimer of MnPcs. These configurations were rarely observed during the experiments and they can be seen as trimers in which a molecule is missing. The similar behavior of MnPcs on the SIC and the MnPcs-induced SIC phase suggests that the molecule-substrate interactions are similar on both surfaces. This observation further confirms that the MnPcs adsorption on top of the Pb monolayer actually transforms the $\sqrt{7} \times \sqrt{3}$-Pb phase into the SIC phase.

In summary, at low coverage MnPc molecules deposited on the $\sqrt{7} \times \sqrt{3}$-Pb monolayer induce a surface reconstruction into the incommensurate SIC phase. The above data show that molecules form strong and local bonds with the substrate such that even if they diffuse during deposition, the molecules do not find the required adsorption sites on the incommensurate phase to form large and ordered assemblies. This forces the molecules to lie isolated or in trimers and always in configurations that reflect the threefold symmetry of the Pb surface.

Computational results

To elucidate the details of the macroscopic $\sqrt{7} \times \sqrt{3}$ to SIC structural phase transition of the Pb monolayer induced by MnPc molecules adsorption we performed DFT calculations. Here, one should keep in mind that the SIC phase is an incommensurate surface reconstruction and it cannot be exactly treated with electronic-structure calculations. This is the reason why we assumed a commensurate $\sqrt{3} \times \sqrt{3}$-Pb atomic arrangement instead of the actual incommensurate SIC phase. Note that this simplification is commonly done to address the SIC electronic properties with DFT methods.[10,26,39,44] We did two separate calculations, first the adsorption of a single MnPc molecule onto the $\sqrt{7} \times \sqrt{3}$ phase and second, onto

the $\sqrt{3} \times \sqrt{3}$ phase. The minimum-energy conformations of the two systems are displayed in figure 4.

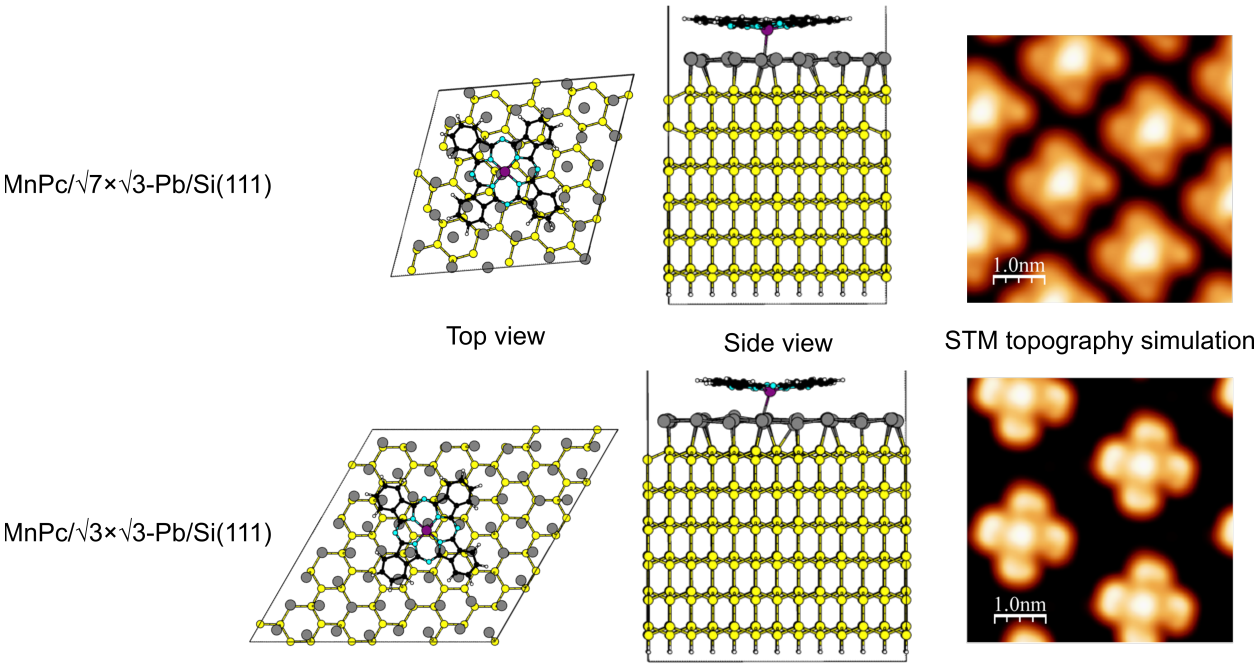

Figure 4: DFT optimized structure and Tersoff-Hamann STM topography[45–47] at fixed current and V_{bias}=+100 mV of a MnPc molecule adsorbed onto the $\sqrt{7} \times \sqrt{3}$-Pb layer on Si(111) (top) and $\sqrt{3} \times \sqrt{3}$-Pb layer on Si(111) (bottom). Supercell dimensions are $22.46 \times 19.9 \times 38.8$ Å^3 and $27.45 \times 26.65 \times 38.8$ Å^3 for top views and side views respectively. C, H, N, Mn, Pb and Si atoms are modelled with black, white, light blue, purple, grey and yellow balls respectively. Both adsorbed molecules are located nearby atop positions above the Pb layer and display a pronounced tilt of each leg of about 8-9°independently of the substrate due to the newly formed Mn-Pb bond. This tilt is only about 3° in gas phase. But Mn-Pb closest distances are different: 2.9 Å for $\sqrt{7} \times \sqrt{3}$-Pb/Si(111) and 2.7 Å for $\sqrt{3} \times \sqrt{3}$-Pb/Si(111), in agreement with 120 meV larger molecular adsorption energy for the latter case.

Our DFT calculations permit to reproduce the known features of the two Pb monoatomic-layer phases on Si(111). The top view of figure 4 shows the adsorbed MnPc molecule on $\sqrt{7} \times \sqrt{3}$-Pb. The unit cell of the surface without the molecule contains 6 Pb atoms per 5 Si atoms corresponding to the Pb coverage of $\frac{6}{5}$ ML=1.2 ML.[25,29,31,33,35,36] Five of these Pb atoms form covalent-like bonds with the underlying Si atoms thus saturating all the dangling bonds and stabilizing the commensurate phase. Due to the *sp*-character of the Pb electronic structure at the Fermi energy, this monoatomic layer presents very small corru-

gation as well as a confined 2D electronic structure.[10,29–31,33,35,36] Figure 4 also shows the top view of the adsorbed MnPc molecule on $\sqrt{3} \times \sqrt{3}$-Pb. The surface unit cell without molecule contains 4 Pb atoms per 3 Si atoms corresponding to the above-mentioned coverage of $\frac{4}{3}$ ML=1.33 ML.[22,34,38,41,42] Covalent bonds between Pb atoms and underlying Si substrate help to stabilize the surface reconstruction whereas Pb-Pb metallic bonds make the SIC phase metallic with 2D electronic properties.[10,29,30,33]

Upon molecular adsorption, there is no major distortion of the underlying Pb layer: the Pb atoms are only slightly displaced on both substrates (see figure S1 in Supporting Information). Interestingly, the alignment of the MnPc molecule with respect to the $\sqrt{3} \times \sqrt{3}$-Pb phase agrees with that experimentally observed in the STM images. The local conformation of the molecule is very similar on the two phases. The Mn atom approaches a Pb atom, responsible for the in-plane metallic bonds, favoring nearby on top adsorption, but also presents electronic hybridization with the passivated Si adatom underneath. This leads to a rather local and strong bond with the surface. The ligands largely interact *via* van der Waals forces included by the Tkatchenko and Scheffler scheme in our calculations.[48] As a consequence, the ligands separate from the substrate leading to cup-shape molecular conformations created by the shorter Mn-surface bond. The computed STM images reproduce the main experimental features of MnPc on the Pb monolayer at several voltage biases: for large tunneling resistance we observe a larger height variation at the central Mn atom than on the square-shape ligands. This gives us confidence in the correctness of the found conformations. Quantitative analysis of computational results has allowed us to find that the MnPc adsorption energies are much different for the two surfaces. The energy gain on the $\sqrt{3} \times \sqrt{3}$-Pb phase is larger than on the $\sqrt{7} \times \sqrt{3}$-Pb phase with -2.86 eV adsorption energy versus -2.74 eV respectively. This is in agreement with the shorter bonding distance calculated on the $\sqrt{3} \times \sqrt{3}$-Pb phase. Moreover, the stronger adsorption is associated to a larger charge transfer from the Pb overlayer to the Mn complex. From a Bader analysis,[49] we infer that one MnPc molecule gains 1.2 electrons when it adsorbs on the $\sqrt{3} \times \sqrt{3}$-Pb phase and only

0.78 electrons on the $\sqrt{7}\times\sqrt{3}$-Pb phase. The stronger interaction on the $\sqrt{3}\times\sqrt{3}$-Pb phase

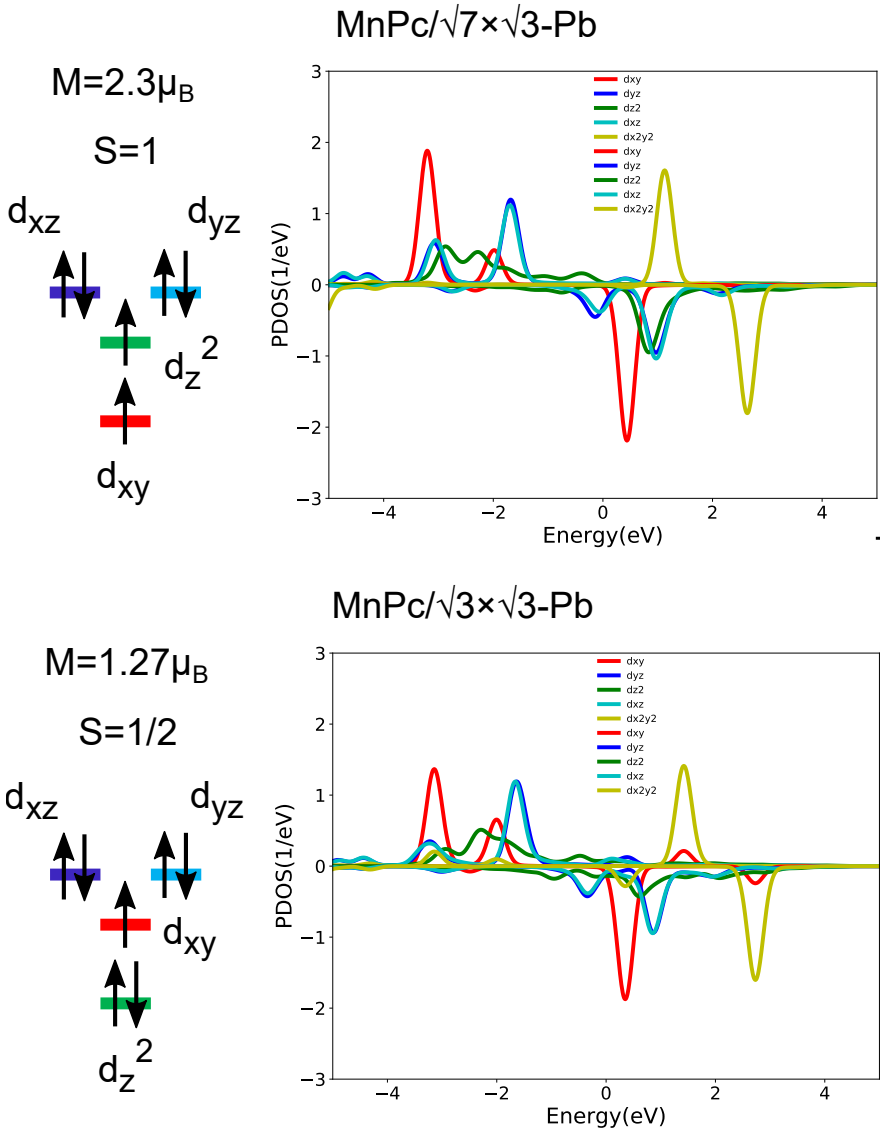

Figure 5: Projected spin-polarized Density of States onto the d-orbitals of the Mn atom and derived ligand-field splitting scheme of Mn d-levels.

leads to a different electronic configuration of the molecule on the two surfaces. From the spin-polarized projected density of states (PDOS) displayed in figure 5, we can derive the corresponding ligand-field d-shell splitting cartoon: there are respectively 2 and 1 unpaired electrons for the $\sqrt{7}\times\sqrt{3}$-Pb and the $\sqrt{3}\times\sqrt{3}$-Pb monolayer. In agreement with previous works, our calculations for a MnPc molecule in the gas phase yield an electronic configuration with a spin S=3/2.[50–53] However, after adsorption on the $\sqrt{7}\times\sqrt{3}$-Pb phase, our calculations

reveal that the total molecular spin decreases from S=3/2 to S=1 as a result of charge transfer to the d_{xz}/d_{yz} orbitals that are hybridized with the ligand orbitals of the MnPc molecule. The S=1 state is ultimately given by the half-occupied d_{z^2} and d_{xy} orbitals (see figure 5). It should be pointed out that the computed electronic structure of the MnPc adsorbed on the $\sqrt{7} \times \sqrt{3}$-Pb monolayer is qualitatively similar to the one identified by Minamitani *et al.*[53] for a MnPc adsorbed on Pb(111) or on a Pb island thick enough to mimic bulk properties. In contrast, the molecular magnetic moment is further reduced on the $\sqrt{3} \times \sqrt{3}$-Pb layer because the d_{z^2} orbital fills as a consequence of larger charge transfer. According to this the d_{z^2} orbital should become non-magnetic. Accordingly, the total molecular spin is expected to be S=1/2 and arise from the only magnetic orbital that is left half-occupied, *i.e.* the d_{xy} orbital. This orbital interacts weakly with the Pb/Si(111) monolayer and its occupation remains essentially unchanged, that is with roughly one unpaired electron.

In summary, our DFT analysis sheds light on the driving force of the MnPcs-induced $\sqrt{7} \times \sqrt{3} \rightarrow$ SIC structural phase transition of the Pb monolayer. MnPc molecules do stabilize better on a denser Pb phase and favors the reconstruction into an incommensurate phase. The initial Pb arrangement of the $\sqrt{7} \times \sqrt{3}$-Pb phase proceeds towards a reorganization to locally form denser areas of $\sqrt{3} \times \sqrt{3}$-Pb and other areas with Pb troughs leading to the overall incommensurate SIC surface structure. In addition, the well-known fact that Pb adatoms in the overlayer are soft and easily mobile[37,39] might help facilitating this process.

Discussion

The present LEED/STM study reveals a new long-range effect taking place when MnPc molecules are adsorbed at low coverage on a Pb/Si(111) monolayer. In particular, we have shown that the adsorption of a very dilute amount of MnPcs is sufficient for Pb atoms initially arranged in the $\sqrt{7} \times \sqrt{3}$-Pb phase to reorganize themselves into the SIC phase on a macroscopic scale. On this MnPcs-induced SIC surface, the molecules remain either isolated or self-assembled in trimers and their adsorption configuration reflects the threefold

symmetry of the substrate. Moreover, our DFT calculations have shown that both the energy gain and the charge transfer of single MnPc molecules adsorbed on a pure $\sqrt{3}\times\sqrt{3}$-Pb phase are larger than on the $\sqrt{7}\times\sqrt{3}$-Pb phase supporting the experimentally observed structural transition.

Adsorption of MnPcs on Pb: 3D vs 2D substrate

In order to get more insight on the link between substrate dimensionality and molecule-substrate coupling strength, we compare below our results with those already reported for adsorption of MPc molecules on 3D substrates. Adsorption of MnPcs on Pb(111) has already been extensively investigated. However, none of these studies has ever reported anything similar to what we observed on the Pb monolayer.

MnPcs deposited on Pb(111) self-assemble in close-packed square lattices even at submonolayer coverage suggesting that their self-assembly is essentially driven by the molecule-molecule interaction as well as the fourfold symmetry of the molecules themselves.[14–16,43] The weak molecule-substrate coupling manifests itself by the emergence of different superstructures superimposed on the square lattice of MnPcs.[15,16,54] The small modulations of this weak molecule-substrate coupling arise from the incommensurability of a square lattice on the triangular Pb(111) surface leading MnPcs to lie on different adsorption sites.[15,43] In stark contrast to these results, our experiments reveal that MnPcs deposited on the Pb monolayer remain either isolated or self-assembled in trimers and their adsorption configurations reflect the threefold symmetry of the SIC phase. This observation seems to suggest that the lower is the dimensionality of the Pb substrate the stronger becomes the molecule-substrate interaction. This statement is supported by the values of adsorption energy (bonding distance) obtained by our DFT analysis, *i.e.* -2.86 eV (2.7 Å) and -2.74 eV (2.9 Å), which are higher (shorter) than those previously reported for a MnPc molecule adsorbed on bulk Pb(111), *i.e.* -1.52 eV[16] (3.29 Å[53]). The computed spatial distribution of the electronic charge and spin density also underlines this strong interface effect: both densities accumulate heavily

on the Si atoms underneath the Pb layer (see figure S2 in Supporting Information). In this sense, the reduced dimensionality of the Pb monolayer permits a direct interaction of the MnPc molecule with the Pb/Si interface, leading to stronger and more localized bonds than on higher dimensional Pb substrates. For example, the recent calculations of Minamitani *et al.*[53] of a single MnPc molecule adsorbed on 3D Pb(111), show that the spin density remains distributed around the molecule and does not penetrate the Pb substrate, in contrast to the present calculations.

We would also like to discuss the interesting case of Au(111), Ag(111) and Cu(111) 3D substrates, all having 2D surface states at the Fermi level, where the adsorption of MPcs leads to isolated molecules[16,54–57] instead of the close-packed self-assembly observed on bulk Pb(111). This behavior has similarities with the present study where we found a reduction of the molecular packing on the Pb monoatomic layers. On coinage metals, the absence of dense assemblies was attributed to the residual charge accumulation at the molecule-substrate interface, resulting from an incomplete screening from the bulk electrons and leading to a subsequent electrostatic repulsion between molecules mediated by the screening of 2D surface states. Following this interpretation, we propose that our 2D Pb substrates may screen the residual molecular charges less effectively than the 3D Pb crystals thus promoting single and few-molecule clusters. Furthermore, on the SIC phase the presence of very different areas on the surface, *i.e.* anisotropic $\sqrt{7} \times \sqrt{3}$ stripes and more isotropic $\sqrt{3} \times \sqrt{3}$ patches, leads to selective adsorption of the majority of molecules on specific zones of the phase giving rise to the observed frustrated molecular self-assembly. This mechanism might ultimately be further enhanced by the locality of the MnPc-substrate interaction leading to molecular adsorption only on certain surface sites and preventing dense molecular packing.

Finally, it should be mentioned that MPcs have already been deposited on other 2D metallic systems. In particular, on the $\sqrt{7}\times\sqrt{3}$-In phase of the In/Si(111) bilayer MPcs (M=Mn,Cu) self-assemble in closely packed square lattices. This indicates that, contrary to our observation, the molecule-molecule interaction is dominant in this system. Moreover, no signs of

molecular-induced surface reconstruction were detected in the In/Si(111) bilayer. This fact highlights the peculiarity of our result and suggests that, as discussed below, in addition to the simple fact of having a low dimensional system, the intervention of the Pb/Si(111) interface might play an important role in tuning the balance between molecule-molecule and molecule-substrate interaction.

At present different computational approaches exist to describe the adsorption of a MnPc molecule on bulk Pb(111).[50–53] All studies agree that the MnPc molecule in the gas phase has an electronic configuration that gives rise to a total spin S=3/2. After adsorption on Pb(111), the magnetic orbital the most strongly hybridized with the substrate is the Mn d_{z^2} and any charge transfer always occurs from the Pb(111) substrate to the MnPc molecule. This is in agreement with our findings. Then, depending on the microscopic details included in the model, *e.g.* electron correlations or hybridization, different predictions on the charge transfer and magnetic state of MnPcs after adsorption come out. In agreement with their new STS results, Minamitani *et al.*[53] reported about a collective magnetic state delocalized on the organic ligand and not localized only on the central Mn atom. According to this, they have shown that after adsorption on Pb(111) the total molecular spin decreases from S=3/2 to S=1 due to a charge transfer of 2.33 electrons essentially localized on the organic ligand and a small contribution of the Mn atom with 0.1 electrons. Our DFT analysis agrees with this result and reveals that the magnetism arising from the d_{z^2} orbital survives after adsorption of MnPcs on the $\sqrt{7}\times\sqrt{3}$-Pb monolayer despite its strong hybridization with the substrate while the magnetism arising from d_{xz}/d_{yz} orbitals (that are coupled to the organic ligands) is suppressed by the charge transfer. This result is different from those reported by previous studies in which the total spin reduction to S=1 or even S=1/2 was interpreted as an interaction with substrate/ligands strictly localized on the magnetic Mn atom and not involving organic ligands.[50,51] Jacob *et al.*[52] reported about the correlated electronic structure of MnPc that retains its magnetic state, *i.e.* S=3/2, after adsorption on Pb(111) but that leads to an effective S=1 spin due to strong dynamical fluctuations of charges between

the d_{xz} and d_{yz} orbitals.

Although our DFT results concerning the electronic/magnetic state of MnPc on the $\sqrt{7}\times\sqrt{3}$-Pb monolayer are in qualitative agreement with the interpretation of Minamitani *et al.*[53] for bulk Pb(111), those for the $\sqrt{3}\times\sqrt{3}$-Pb monolayer reveal something different. On the $\sqrt{3}\times\sqrt{3}$-Pb phase, in addition to the charge transfer to the d_{xz}/d_{yz} orbitals that reduces the total molecular spin by $\sim$1/2, there is an additional charge transfer that quenches the spin arising from the d_{z^2} orbital ultimately resulting in a total spin S=1/2 carried by the d_{xy} orbital. This result further confirms the stronger interaction of MnPcs with the $\sqrt{3}\times\sqrt{3}$-Pb phase than with the $\sqrt{7}\times\sqrt{3}$-Pb phase.

Before concluding this section, we discuss the different charge transfers involving MnPc molecules on bulk or low-dimensional metallic substrates. On Au(111) the charge transfer proceeds from MnPc molecules to the substrate.[54] On Ag(111) it goes in the opposite direction[57] as found in our Pb monolayers and in 3D Pb(111). Despite this similarity, in the MnPc/Ag(111) system the charge transfer, *i.e.* 0.5 electrons,[57] is dominated by the organic ligands while on the $\sqrt{3}\times\sqrt{3}$-Pb monolayer it is dominated by the Mn atom. This emphasizes the locality of the interaction. Another interesting case is the adsorption of MPcs (M=Mn and Cu) on the 2D $\sqrt{7}\times\sqrt{3}$-In bilayer grown on Si(111). It revealed that the electron transfer goes from the substrate to the molecules in both cases.[19] However on one hand this charge transfer takes place on the organic ligands for CuPcs and yields 1.55 electrons.[19] On the other hand it is rather localized on the central atom in the case of MnPcs, in agreement with our findings, and yields 1.78 electrons.[19]

The novelty of our result compared to the great variety of molecular behaviors encountered in literature until now is the new self-assembly of MnPcs on the Pb monolayer that reflects a new way of tuning the molecule-substrate coupling by playing with the substrate dimensionality.

MnPcs-induced surface reconstruction of the Pb monolayer

While our work emphasizes a structural phase transition of the Pb monolayer from the $\sqrt{7} \times \sqrt{3}$ to the SIC phase induced by MnPcs, no structural changes were ever reported on bulk Pb(111) or Pb/Si(111) islands. The reason of this may lie in the smaller strain at the Pb(111) surface compared to those within the Pb monolayer. To clarify this fact it is useful to mention that examples of surface modification induced by molecular adsorption can be found on Au(111). Sun *et al.*,[58] for instance, have reported modifications of the herringbone surface reconstruction of Au(111) whose final structure depends on the adsorbed molecule, *i.e.* FePc or perylene. The explanation of this behavior was based on the fact that the herringbone surface reconstruction is itself induced by surface strain. According to this, the charge transfer that accompanies the molecular adsorption induces a change in the surface strain of Au(111) thus driving a new surface reconstruction. Therefore, adsorption of different molecules on Au(111) induces different surface patterns.

However, the molecular-induced surface reconstruction of Au(111) occurs at a molecular coverage of 1 ML. This is in striking contrast with our experiment in which we observed a long-range surface reconstruction of Pb monolayer driven by a dilute amount of MnPcs. We believe that this long-range effect relies on the fact that the Pb monolayer is a particular type of strained surface. Indeed, it was shown that long-range repulsive interactions within the Pb monolayer are responsible for the emergence of a huge number of structural phases.[59] These repulsive interactions are also responsible for macroscopic rearrangement of phases with different symmetries when the Pb coverage is slightly changed. This fact suggests that a local perturbation (even small) of the Pb monolayer may actually be felt on macroscopic distances through variations of the surface strain inside the system.

Another important effect that is well known to occur in proximity of an adsorbed molecule is the charge transfer which induces a redistribution of the surface electrons within the substrate.[58,60,61] A direct consequence of this electronic reorganization is a variation of both surface strain and local atomic arrangement at the molecule-substrate interface. Interest-

ingly, our DFT calculations show that a strong charge transfer takes place from the Pb monolayer to the MnPc molecule. Furthermore, our charge density maps reveal that the transferred charge is mostly accumulated at the Mn-Pb interface (see figure S2 in supporting information).

Taking into account the various features of our surface system we tentatively propose a mechanism behind the macroscopic phase transition of the Pb monolayer induced by MnPcs adsorption. We believe that the charge transfer between Pb and MnPcs may act as local perturbations that affect the surface strain of the whole system and initiate the structural transformation. The $\sqrt{7} \times \sqrt{3} \rightarrow$ SIC phase transition may ultimately be promoted by the energetic stability of the MnPc/SIC system, revealed by our DFT calculations, together with the high mobility of Pb atoms on top of the Si(111). This idea is reinforced by a recent study that reported about a charge transfer-induced structural phase transition of the $\sqrt{3} \times \sqrt{3}$-Au/Si(111) monolayer under adsorption of 0.1 ML of Na atoms.[62,63]

Conclusions

In conclusion, with this study we have shown that the adsorption of a minute amount of MnPc molecules ($\sim$0.18 molecules/100 nm^2) on top of a Pb/Si(111) monolayer kept at 150 K and room temperature induces a structural transition of the $\sqrt{7} \times \sqrt{3}$-Pb phase into the SIC-Pb phase on a macroscopic scale. Analysis of experimental and computational results revealed that the mechanism behind this surface transformation may be related to the strong charge transfer at the molecule/substrate interface as well as the strained nature of the surface reconstructions of the Pb monolayer. As shown by our DFT calculations, the phase transition could ultimately be promoted by the energetic stability of the MnPc/SIC-Pb/Si(111) system with respect to the MnPc/$\sqrt{7} \times \sqrt{3}$-Pb/Si(111) one.

We have also shown that there exists intrinsic differences between the electronic/structural properties of the Pb monolayer and those of thicker Pb substrates that might be ascribed

to the participation of the Pb/Si(111) interface in the molecule-substrate interaction. In particular, a different self-assemblying behavior as well as a different electronic/magnetic state of individual MnPcs was found in the present study. This interesting result opens up the possibility of using the substrate dimensionality to tune the molecule-substrate coupling as well as the electronic and magnetic properties of organic hybrid systems.

Our results can have a strong impact in the search for organized magnetic nanostructures on superconductors. In particular, the rich and new behavior of hybrid organic/metal systems occurring when the dimensionality of the metal substrate is reduced enables a new way of tuning the coupling between single and assembled magnetic molecules and a 2D superconductor. This could be important for research aiming to stabilizing magnetic order in metal-organic systems.

Methods

Sample preparation

All the experiments were carried out in Ultra-High Vacuum (UHV) with a base pressure better than 5×10^{-11} mbar. Heavily n-doped Si(111) substrates were firstly outgassed at 873 K for several hours after being introduced in UHV and then repeatedly flashed at 1420 K by direct current heating. Atomically clean and defect-free Si(111)-7×7 reconstructed surfaces were prepared by repeatedly flashing the Si(111) sample to 1420 K and subsequent annealing from 1220 K to 820 K by slowly decreasing the temperature. Pb was evaporated at a rate of 0.65 ML/min on top of the freshly prepared Si(111)-7×7 surface kept at room temperature from an electron beam evaporator. A crystalline Pb monolayer was finally obtained by annealing the Pb/Si(111) system at about 600 K for a duration that depends on the desired surface reconstruction. In particular, after depositing 1.65 ML of Pb, the $\sqrt{7}\times\sqrt{3}$-Pb and the SIC phase were obtained by annealing the sample at ∼593 K for approximately 2 min 30 sec and 1 min 10 sec respectively. MnPcs were thermally sublimated at about 620 K on top of

the Pb surface kept either at room temperature or at ∼150 K from a home-made resistively heated glass crucible.

STM experiments

Scanning Tunneling Microscopy (STM) measurements were performed *in situ* on a low temperature homemade system. Mechanically cut PtIr tips were used after being outgassed at around 470 K for several hours. All STM images were acquired in constant current mode with the sample kept at 77 K except that in figure 3 that was acquired at 300 mK. STM data were calibrated from high resolution images of the Si(111)-7×7 surface recorded at the same temperature.

DFT calculations

Two adsorption systems were considered in the calculations: a single MnPc molecule adsorbed onto a $\sqrt{3} \times \sqrt{3}$ and a $\sqrt{7} \times \sqrt{3}$ reconstructed Pb overlayer on Si(111) substrate respectively. Bulk Si(111) was modeled by means of a slab consisting of 6 Si bilayers passivated at one end with hydrogen atoms. In both adsorption systems, the atomic positions of the topmost Si bilayer, the top layer of Pb atoms and the MnPc molecule were all relaxed until atomic forces were smaller than 50 meV per Å. The projected spin-polarized density of states (PDOS) onto the d atomic orbitals of the Mn atom used a gaussian smearing with a width of 0.2 eV to smooth the plots. Spin-Polarized DFT calculations were performed for a periodic slab geometry as implemented in the VASP code.[64] A cut-off energy of 280 eV in the plane-wave expansion was used together with a $1 \times 1 \times 1$ k-grid (Γ point) for the geometry optimization. For the static electronic structure calculations like PDOS and STM simulations a finer $3 \times 3 \times 1$ k-grid was adopted together with an increased cut-off energy of 350 eV. The smearing technique using a Gaussian broadening of 0.01 eV was applied to achieve electronic convergence. Exchange and correlation were treated with the PBE form of the generalized gradient approximation.[65] Dispersion interactions were modeled with the

variant of DFT-D3 method by Grimme.[66,67]

Acknowledgement

We gratefully acknowledge F. Thibout (Kastler Brossel Laboratory) for the realization of the glass crucibles used during the experiments of this study. NL gratefully acknowledges financial support from the spanish MICINN (project RTI2018-097895-B-C44) and FEDER funds. NW gratefully acknowlegde the financial support of Labex Matisse and Investissement d'Avenir. CB gratefully acknowledges financial support from the French ANR Rodesis (project ANR-16-CE30-0011-01). The computational work was granted access to the HPC resources of GENCI (TGCC and CINES) under grant n°A0050807364.

Supporting Information Available

Additional figures are available. They show the calculated atomic relaxation of the Pb monolayer after MnPc adsorption and the charge/spin density distributions of a MnPc molecule adsorbed on the $\sqrt{7} \times \sqrt{3}$-Pb and the SIC-Pb phase.

This material is available free of charge *via* the Internet at http://pubs.acs.org

References

1. Nadj-Perge, S.; Drozdov, I. K.; Li, J.; Chen, H.; Jeon, S.; Seo, J.; MacDonald, A. H.; Bernevig, B. A.; Yazdani, A. Observation of Majorana Fermions in Ferromagnetic Atomic Chains on a Superconductor. *Science* **2014**, *346*, 602–607.

2. Yazdani, A.; Jones, B. A.; Lutz, C. P.; Crommie, M. F.; Eigler, D. M. Probing the Local Effects of Magnetic Impurities on Superconductivity. *Science* **1997**, *275*, 1767–1770.

3. Ji, S.-H.; Zhang, T.; Fu, Y.-S.; Chen, X.; Ma, X.-C.; Li, J.; Duan, W.-H.; Jia, J.-

F.; Xue, Q.-K. High-Resolution Scanning Tunneling Spectroscopy of Magnetic Impurity Induced Bound States in the Superconducting Gap of Pb Thin Films. *Phys. Rev. Lett.* **2008**, *100*, 226801.

4. Choi, D.-J.; Rubio-Verdú, C.; de Bruijckere, J.; Ugeda, M. M.; Lorente, N.; Pascual, J. I. Mapping the Orbital Structure of Impurity Bound States in a Superconductor. *Nat. Commun.* **2017**, *8*, 15175.

5. Heinrich, B. W.; Pascual, J. I.; Franke, K. J. Single Magnetic Adsorbates on S-Wave Superconductors. *Prog. Surf. Sci.* **2018**, *93*, 1–19.

6. Ménard, G. C.; Guissart, S.; Brun, C.; Pons, S.; Stolyarov, V. S.; Debontridder, F.; Leclerc, M. V.; Janod, E.; Cario, L.; Roditchev, D.; Simon, P.; Cren, T. Coherent Long-Range Magnetic Bound States in a Superconductor. *Nat. Phys.* **2015**, *11*, 1013–1016.

7. Ménard, G. C.; Guissart, S.; Brun, C.; Leriche, R. T.; Trif, M.; Debontridder, F.; Demaille, D.; Roditchev, D.; Simon, P.; Cren, T. Two-Dimensional Topological Superconductivity in Pb/Co/Si(111). *Nat. Commun.* **2017**, *8*, 2040.

8. Kezilebieke, S.; Dvorak, M.; Ojanen, T.; Liljeroth, P. Coupled Yu–Shiba–Rusinov States in Molecular Dimers on $NbSe_2$. *Nano Lett.* **2018**, *18*, 2311–2315.

9. Ménard, G. C.; Mesaros, A.; Brun, C.; Debontridder, F.; Roditchev, D.; Simon, P.; Cren, T. Isolated Pairs of Majorana Zero Modes in a Disordered Superconducting Lead Monolayer. *Nat. Commun.* **2019**, *10*, 2587.

10. Zhang, T.; Cheng, P.; Li, W.-J.; Sun, Y.-J.; Wang, G.; Zhu, X.-G.; He, K.; Wang, L.; Ma, X.; Chen, X.; Wang, Y.; Liu, Y.; Lin, H.-Q.; Jia, J.-F.; Xue, Q.-K. Superconductivity in One-Atomic-Layer Metal Films Grown on Si(111). *Nat. Phys.* **2010**, *6*, 104–108.

11. Brun, C.; Cren, T.; Cherkez, V.; Debontridder, F.; Pons, S.; Fokin, D.; Tringides, M. C.; Bozhko, S.; Ioffe, L. B.; Altshuler, B. L.; Roditchev, D. Remarkable Effects of Disorder

on Superconductivity of Single Atomic Layers of Lead on Silicon. *Nat. Phys.* **2014**, *10*, 444–450.

12. Brun, C.; Cren, T.; Roditchev, D. Review of 2D Superconductivity: the Ultimate Case of Epitaxial Monolayers. *Supercond. Sci. Technol.* **2017**, *30*, 013003.

13. Gargiani, P.; Rossi, G.; Biagi, R.; Corradini, V.; Pedio, M.; Fortuna, S.; Calzolari, A.; Fabris, S.; Cezar, J. C.; Brookes, N. B.; Betti, M. G. Spin and Orbital Configuration of Metal Phthalocyanine Chains Assembled on the Au(110) Surface. *Phys. Rev. B* **2013**, *87*, 165407.

14. Shuai-Hua, J.; Ying-Shuang, F.; Tong, Z.; Xi, C.; Jin-Feng, J.; Qi-Kun, X.; Xu-Cun, M. Kondo Effect in Self-Assembled Manganese Phthalocyanine Monolayer on Pb Islands. *Chin. Phys. Lett.* **2010**, *27*, 087202.

15. Hao, D.; Song, C.; Ning, Y.; Wang, Y.; Wang, L.; Ma, X.-C.; Chen, X.; Xue, Q.-K. Self-Assembly of Manganese Phthalocyanine on Pb(111) Surface: a Scanning Tunneling Microscopy Study. *J. Chem. Phys* **2011**, *134*, 154703.

16. Jiang, Y. H.; Xiao, W. D.; Liu, L. W.; Zhang, L. Z.; Lian, J. C.; Yang, K.; Du, S. X.; Gao, H.-J. Self-Assembly of Metal Phthalocyanines on Pb(111) and Au(111) Surfaces at Submonolayer Coverage. *J. Phys. Chem C* **2011**, *115*, 21750–21754.

17. Yang, K.; Xiao, W. D.; Jiang, Y. H.; Zhang, H. G.; Liu, L. W.; Mao, J. H.; Zhou, H. T.; Du, S. X.; Gao, H.-J. Molecule–Substrate Coupling between Metal Phthalocyanines and Epitaxial Graphene Grown on Ru(0001) and Pt(111). *J. Phys. Chem. C* **2012**, *116*, 14052–14056.

18. Liu, L. W.; Yang, K.; Xiao, W. D.; Jiang, Y. H.; Song, B. Q.; Du, S. X.; Gao, H.-J. Selective Adsorption of Metal-Phthalocyanine on Au(111) Surface with Hydrogen Atoms. *Appl. Phys. Lett.* **2013**, *103*, 023110.

19. Yoshizawa, S.; Minamitani, E.; Vijayaraghavan, S.; Mishra, P.; Takagi, Y.; Yokoyama, T.; Oba, H.; Nitta, J.; Sakamoto, K.; Watanabe, S.; Nakayama, T.; Uchihashi, T. Controlled Modification of Superconductivity in Epitaxial Atomic Layer–Organic Molecule Heterostructures. *Nano Lett.* **2017**, *17*, 2287–2293.

20. Suzuki, T.; Lawrence, J.; Morbec, J. M.; Kratzer, P.; Costantini, G. Surface Structural Transition Induced by the Formation of Metal-Organic Networks on the Si(111)-$\sqrt{7}\times\sqrt{3}$-In Surface. *Nanoscale* **2019**, *11*, 21790–21798.

21. Matetskiy, A. V.; Bondarenko, L. V.; Gruznev, D. V.; Zotov, A. V.; Saranin, A. A.; Tringides, M. C. Structural Transformations in Pb/Si(111) Phases Induced by C_{60} Adsorption. *J. Phys.: Condens. Matter* **2013**, *25*, 395006.

22. Horikoshi, K.; Tong, X.; Nagao, T.; Hasegawa, S. Structural Phase Transitions of Pb-adsorbed Si(111) Surfaces at Low Temperatures. *Phys. Rev. B* **1999**, *60*, 13287.

23. Slezák, J.; Mutombo, P.; Cháb, V. STM Study of a Pb/Si(111) Interface at Room and Low Temperatures. *Phys. Rev. B* **1999**, *60*, 13328.

24. Custance, O.; Gómez-Rodríguez, J. M.; Baró, A. M.; Juré, L.; Mallet, P.; Veuillen, J.-Y. Low Temperature Phases of Pb/Si(111). *Surf. Sci.* **2001**, *482*, 1399–1405.

25. Brochard, S.; Artacho, E.; Custance, O.; Brihuega, I.; Baró, A. M.; Soler, J. M.; Gómez-Rodríguez, J. M. *Ab Initio* Calculations and Scanning Tunneling Microscopy Experiments of the Si(111)-($\sqrt{7}\times\sqrt{3}$)-Pb Surface. *Phys. Rev. B* **2002**, *66*, 205403.

26. Chan, T.-L.; Wang, C. Z.; Hupalo, M.; Tringides, M. C.; Lu, Z.-Y.; Ho, K. M. First-Principles Studies of Structures and Stabilities of Pb/Si(111). *Phys. Rev. B* **2003**, *68*, 045410.

27. Stepanovsky, S.; Yakes, M.; Yeh, V.; Hupalo, M.; Tringides, M. C. The Dense α-$\sqrt{3}\times$

$\sqrt{3}$Pb/Si(111) Phase: A Comprehensive STM and SPA-LEED Study of Ordering, Phase Transitions and Interactions. *Surf. Sci.* **2006**, *600*, 1417–1430.

28. Cudazzo, P.; Profeta, G.; Continenza, A. Low Temperature Phases of Pb/Si(111) and Related Surfaces. *Surf. Sci* **2008**, *602*, 747–754.

29. Jung, S. C.; Kang, M. H. Dynamical Nature of the High-Temperature Pb/Si(111)-1×1 Phase. *Phys. Rev. B* **2011**, *84*, 155422.

30. Choi, W. H.; Koh, H.; Rotenberg, E.; Yeom, H. W. Electronic Structure of Dense Pb Overlayers on Si(111) Investigated Using Angle-resolved Photoemission. *Phys. Rev. B* **2007**, *75*, 075329.

31. Hsu, C.-H.; Chuang, F.-C.; Albao, M. A.; Yeh, V. Electronic Structure of the Pb/Si(111)-($\sqrt{7} \times \sqrt{3}$) Surface Reconstruction: a First-Principles Study. *Phys. Rev. B* **2010**, *81*, 033407.

32. Kim, K. S.; Jung, S. C.; Kang, M. H.; Yeom, H. W. Nearly Massless Electrons in the Silicon Interface with a Metal Film. *Phys. Rev. Lett.* **2010**, *104*, 246803.

33. Jung, S. C.; Kang, M. H. Triple-Domain Effects on the Electronic Structure of Pb/Si(111)-($\sqrt{7}\times\sqrt{3}$): Density-Functional Calculations. *Surf. Sci.* **2011**, *605*, 551–554.

34. Ganz, E.; Hwang, I.-S.; Xiong, F.; Theiss, S. K.; Golovchenko, J. Growth and Morphology of Pb on Si(111). *Surf. Sci.* **1991**, *257*, 259–273.

35. Choi, W. H.; Kim, K. S.; Yeom, H. W. High-Resolution Core-Level Photoemission Study of Dense Pb Overlayers on Si(111). *Phys. Rev. B* **2008**, *78*, 195425.

36. Kumpf, C.; Bunk, O.; Zeysing, J. H.; Nielsen, M. M.; Nielsen, M.; Johnson, R. L.; Feidenhans'l, R. Structural Study of the Commensurate–Incommensurate Low-Temperature Phase Transition of Pb on Si(111). *Surf. Sci.* **2000**, *448*, L213–L219.

37. Hupalo, M.; Schmalian, J.; Tringides, M. C. "Devil's Staircase" in Pb/Si(111) Ordered Phases. *Phys. Rev. Lett.* **2003**, *90*, 216106.

38. Seehofer, L.; Falkenberg, G.; Daboul, D.; Johnson, R. L. Structural Study of the Close-packed Two-Dimensional Phases of Pb on Ge(111) and Si(111). *Phys. Rev. B* **1995**, *51*, 13503.

39. Hupalo, M.; Chan, T. L.; Wang, C. Z.; Ho, K. M.; Tringides, M. C. Atomic Models, Domain-Wall Arrangement, and Electronic Structure of the Dense Pb/Si(111)-$\sqrt{3} \times \sqrt{3}$ Phase. *Phys. Rev B* **2002**, *66*, 161410(R).

40. Li, W.-J.; Sun, Y.-J.; Zhang, T.; Zhu, X.-G.; Wang, G.; Jia, J.-F.; Ma, X.; Chen, X.; Xue, Q.-K. Enhancement of Superconductivity of Pb Ultra-Thin Films by the Interface Effect. *Surf. Rev. Lett.* **2010**, *17*, 437–440.

41. Hwang, I.-S.; Martinez, R. E.; Liu, C.; Golovchenko, J. A. Soft Incommensurate Reconstruction on Pb/Si(111): Structure, Stress Modulation, and Phase Transition. *Phys. Rev. B* **1995**, *51*, 10193.

42. Petkova, A.; Wollschläger, J.; Günter, H.-L.; Henzler, M. Formation and Commensurate Analysis of "Incommensurate" Superstructures of Pb on Si(111). *Surf. Sci.* **2001**, *471*, 11–20.

43. Franke, K. J.; Schulze, G.; Pascual, J. I. Competition of Superconducting Phenomena and Kondo Screening at the Nanoscale. *Science* **2011**, *332*, 940–944.

44. Ren, X.-Y.; Kim, H.-J.; Yi, S.; Jia, Y.; Cho, J.-H. Spin-Orbit Coupling Effects on the Stability of Two Competing Structures in Pb/Si(111) and Pb/Ge(111). *Phys. Rev. B* **2016**, *94*, 075436.

45. Tersoff, J.; Hamann, D. R. Theory of the Scanning Tunneling Microscope. *Phys. Rev. B* **1985**, *31*, 805.

46. Bocquet, M.-L.; Lesnard, H.; Monturet, S.; Lorente, N. *Computational Methods in Catalysis and Materials Science*; Wiley-Blackwell, 2009; pp 199–219.

47. Lorente, N.; Robles, R. STMpw, (Version v1.0b2). 2019; `http://doi.org/10.5281/zenodo.3581159`.

48. Tkatchenko, A.; Scheffler, M. Accurate Molecular Van Der Waals Interactions from Ground-State Electron Density and Free-Atom Reference Data. *Phys. Rev. Lett.* **2009**, *102*, 073005.

49. Tang, W.; Sanville, E.; Henkelman, G. A Grid-based Bader Analysis Algorithm Without Lattice Bias. *J. Phys. Condens. Matter* **2009**, *21*, 084204.

50. Fu, Y.-S.; Ji, S.-H.; Chen, X.; Ma, X.-C.; Wu, R.; Wang, C.-C.; Duan, W.-H.; Qiu, X.-H.; Sun, B.; Zhang, P.; Jia, J.-F.; Xue, Q.-K. Manipulating the Kondo Resonance Through Quantum Size Effects. *Phys. Rev. Lett.* **2007**, *99*, 256601.

51. Bauer, J.; Pascual, J. I.; Franke, K. J. Microscopic Resolution of the Interplay of Kondo Screening and Superconducting Pairing: Mn-Phthalocyanine Molecules Adsorbed on Superconducting Pb(111). *Phys. Rev. B* **2013**, *87*, 075125.

52. Jacob, D.; Soriano, M.; Palacios, J. J. Kondo Effect and Spin Quenching in High-Spin Molecules on Metal Substrates. *Phys. Rev. B* **2013**, *88*, 134417.

53. Minamitani, E.; Fu, Y.-S.; Xue, Q.-K.; Kim, Y.; Watanabe, S. Spatially Extended Underscreened Kondo State from Collective Molecular Spin. *Phys. Rev. B* **2015**, *92*, 075144.

54. Jiang, Y.-H.; Liu, L.-W.; Yang, K.; Xiao, W.-D.; Gao, H.-J. Self-Assembly and Growth of Manganese Phthalocyanine on an Au(111) Surface. *Chin. Phys. B* **2011**, *20*, 096401.

55. Cheng, Z. H.; Gao, L.; Deng, Z. T.; Liu, Q.; Jiang, N.; Lin, X.; He, X. B.; Du, S. X.; Gao, H.-J. Epitaxial Growth of Iron Phthalocyanine at the Initial Stage on Au(111) Surface. *J. Phys. Chem. C* **2007**, *111*, 2656–2660.

56. Snezhkova, O.; Bischoff, F.; He, Y.; Wiengarten, A.; Chaudhary, S.; Johansson, N.; Schulte, K.; Knudsen, J.; Barth, J. V.; Seufert, K.; Auwärter, W.; Schnadt, J. Iron Phthalocyanine on Cu(111): Coverage-dependent Assembly and Symmetry Breaking, Temperature-induced Homocoupling, and Modification of the Adsorbate-Surface Interaction by Annealing. *J. Chem. Phys.* **2016**, *144*, 094702.

57. Tuerhong, R.; Ngassam, F.; Watanabe, S.; Onoe, J.; Alouani, M.; Bucher, J.-P. Two-Dimensional Organometallic Kondo Lattice with Long-Range Antiferromagnetic Order. *J. Phys. Chem. C* **2018**, *122*, 20046–20054.

58. Sun, J. T.; Gao, L.; He, X. B.; Cheng, Z. H.; Deng, Z. T.; Lin, X.; Hu, H.; Du, S. X.; Liu, F.; Gao, H.-J. Surface Reconstruction Transition of Metals Induced by Molecular Adsorption. *Phys. Rev. B* **2011**, *83*, 115419.

59. Yakes, M.; Hupalo, M.; Zaluska-Kotur, M. A.; Gortel, Z. W.; Tringides, M. C. Low-Temperature Ultrafast Mobility in Systems with Long-Range Repulsive Interactions: Pb / Si (111). *Phys. Rev. Lett.* **2007**, *98*, 135504.

60. Ibach, H. The Role of Surface Stress in Reconstruction, Epitaxial Growth and Stabilization of Mesoscopic Structures. *Surf. Sci. Rep.* **1997**, *29*, 195–263.

61. Tseng, T.-C.; Urban, C.; Wang, Y.; Otero, R.; Tait, S. L.; Alcamí, M.; Écija, D.; Trelka, M.; Gallego, J. M.; Lin, N.; Konuma, M.; Starke, U.; Nefedov, A.; Langner, A.; Wöll, C.; Herranz, M. Á.; Martín, F.; Martín, N.; Kern, K.; Miranda, R. Charge-Transfer-induced Structural Rearrangements at Both Sides of Organic/Metal Interfaces. *Nat. Chem.* **2010**, *2*, 374–379.

62. Bondarenko, L. V.; Gruznev, D. V.; Yakovlev, A. A.; Tupchaya, A. Y.; Usachov, D.; Vilkov, O.; Fedorov, A.; Vyalikh, D. V.; Eremeev, S. V.; Chulkov, E. V.; Zotov, A. V.; Saranin, A. A. Large Spin Splitting of Metallic Surface-State Bands at Adsorbate-modified Gold/Silicon Surfaces. *Sci. Rep.* **2013**, *3*, 1826.

63. Bondarenko, L. V.; Matetskiy, A. V.; Yakovlev, A. A.; Tupchaya, A. Y.; Gruznev, D. V.; Ryzhkova, M. V.; Tsukanov, D. A.; Borisenko, E. A.; Chukurov, E. N.; Denisov, N. V.; Vilkov, O.; Vyalikh, D. V.; Zotov, A. V.; Saranin, A. A. Effect of Na Adsorption on the Structural and Electronic Properties of Si(111)$\sqrt{3} \times \sqrt{3}$-Au Surface. *J. Phys.: Condens. Matter* **2014**, *26*, 055009.

64. Kresse, G.; Furthmüller, J. Efficiency of *Ab-Initio* Total Energy Calculations for Metals and Semiconductors Using a Plane-Wave Basis Set. *Comput. Mater. Sci.* **1996**, *6*, 15–50.

65. Perdew, J. P.; Burke, K.; Ernzerhof, M. Generalized Gradient Approximation Made Simple. *Phys. Rev. Lett.* **1996**, *77*, 3865.

66. Grimme, S.; Antony, J.; Ehrlich, S.; Krieg, H. A Consistent and Accurate *Ab Initio* Parametrization of Density Functional Dispersion Correction (DFT-D) for the 94 Elements H-Pu. *J. Chem. Phys.* **2010**, *132*, 154104.

67. Grimme, S.; Ehrlich, S.; Goerigk, L. Effect of the Damping Function in Dispersion Corrected Density Functional Theory. *J. Comput. Chem.* **2011**, *32*, 1456–1465.

Graphical TOC Entry